



**ARTICLE**

# Flame Retardant Material Based on Cellulose Scaffold Mineralized by Calcium Carbonate

Jinshuo Wang, Lida Xing, Fulong Zhang and Chuanfu Liu\*

State Key Laboratory of Pulp and Paper Engineering, School of Light Industry and Engineering, South China University of Technology, Guangzhou, 510640, China

\*Corresponding Author: Chuanfu Liu. Email: chfliu@scut.edu.cn

Received: 30 January 2023 Accepted: 13 March 2023 Published: 23 January 2024

## ABSTRACT

Wood-based functional materials have developed rapidly. But the flammability significantly limits its further application. To improve the flame retardancy, the balsa wood was delignified by  $\text{NaClO}_2$  solution to create a cellulose scaffold, and then alternately immersed in  $\text{CaCl}_2$  ethanol solution and  $\text{NaHCO}_3$  aqueous solution under vacuum. The high porosity and wettability resulting from delignification benefited the following mineralization process, changing the thermal properties of balsa wood significantly. The organic-inorganic wood composite showed abundant  $\text{CaCO}_3$  spherical particles under scanning electron microscopy. The peak of the heat release rate of delignified balsa- $\text{CaCO}_3$  was reduced by 33% compared to the native balsa, according to the cone calorimetric characterization. The flame test demonstrated that the mineralized wood was flame retardant and self-extinguish. Additionally, the mineralized wood also displayed lower thermal conductivity. This study developed a feasible way to fabricate a lightweight, fire-retardant, self-extinguishing, and heat-insulating wood composite, providing a promising route for the valuable application of cellulosic biomass.

## KEYWORDS

Cellulose scaffold; delignification;  $\text{CaCO}_3$ ; mineralization; fire retardancy

## 1 Introduction

Wood is widely used as a cellulosic material, as it is mechanically strong, highly porous, cost-effective, and environmentally friendly [1,2]. However, woody biomass is also highly flammable, which significantly limits its utilization scenario [3,4]. Surface-coating of fire-retardant additives is able to improve fire resistance [5]. But it required renovation with time because of its instability. Another issue is that many flame retardants are detrimental to human health [6,7]. Halogen-free flame retardants are the future development direction, such as silicon flame retardants [8] and intumescent flame retardants [9], which are widely used in the preparation of flame retardant polymer materials. But most strategies struggle to penetrate into the interior of the wood. Therefore, it is desperate to develop an environmentally friendly and efficient method to address the flammable issue of wood materials.

Recently, wood mineralization concepts have been used for multifunctional hybrid organic/inorganic materials [10,11].  $\text{CaCO}_3$ , as a commonly used mineral, is environmentally friendly and highly efficient in gas-phase flame retardancy. It absorbs part of the heat by thermal decomposition and releases  $\text{CO}_2$  to



dilute the flammable volatiles and oxygen concentration in the flame [12,13]. Merk et al. successfully introduced  $\text{CaCO}_3$  into the cell wall and produced a mineralized wood [14]. Pondelak et al. impregnated the wood with a calcium acetoacetate aqueous solution and then controlled the temperature and humidity to generate the  $\text{CaCO}_3$  particles in the wood cell wall [15]. However, both of these methods are of low efficiency to attain a sufficient level of mineralization that is able to improve fire resistance, because the compact structure of wood block limited the diffusion of calcium salt solution.

Partial removal of lignin from wood is able to expose more cellulose and meanwhile retain the native scaffold of wood, therefore increasing the porosity and benefiting the downstream functionalization of the wood materials [16,17]. Several groups reported the preparation of a variety of functional materials, such as structural materials [18–21], transparent wood [22,23], electromagnetic-interference shielding materials [24], and energy storage materials [25], based on the partially delignified wood block. Fu et al. introduced the montmorillonite clay nanoplatelets inside the cell walls of delignified wood scaffolds using hydrocolloidal suspensions and obtained fire-retardant wood hybrids [26]. Zhang et al. infiltrated the  $\text{Ti}_3\text{C}_2\text{T}_x$  (MXene) into delignified wood to prepare MXene-reinforced transparent wood [27]. Inspired by these studies, we supposed that delignification could significantly increase the diffusion rate of calcium in the cell wall and enhance the efficiency of mineralization, therefore resulting in a fire-retardant woody material.

Herein, we developed a “top-down” approach to preparing a flame-retardant material. The native balsa wood was partially delignified by  $\text{NaClO}_2$  to create the cellulose scaffold. The oriented fiber structure of wood was preserved. Then by employing alternating solution-exchange cycles with  $\text{CaCl}_2$  in ethanol and  $\text{NaHCO}_3$  in water, the mineral precipitation can be achieved. Partial delignification led to better wettability and higher porosity, increasing the diffusion and absorption rate of calcium salt and improving the level of mineralization. The resulting mineralized wood displayed great flame retardancy and self-extinguishing, which was of great potential as energy efficient building materials or sandwich materials.

## 2 Experimental Part

### 2.1 Materials and Chemicals

Balsa wood was purchased from a local factory in Guangzhou. It was cut into chips with the dimensions of 50 mm × 50 mm × 3 mm (axial × tangential × radial). Sodium chlorite ( $\text{NaClO}_2$ , 80%), and sodium bicarbonate ( $\text{NaHCO}_3$ ) were purchased from Macklin. Anhydrous calcium chloride ( $\text{CaCl}_2$ ) was purchased from Guangzhou Jinhua Chemical Reagent Co., Ltd., China.

### 2.2 Delignification and Mineralization

The wood chips were put in the 2%  $\text{NaClO}_2$  solution. The pH value was adjusted to 4.6 by acetic acid. The solution was then heated to 80°C for 8 h. After treatment, the balsa chips were thoroughly washed using deionized water to remove the residual chemicals.

The mineralization was performed using a circulating water vacuum pump and a vacuum dryer. Both the native and delignified wood samples were immersed in  $\text{CaCl}_2$  ethanol solution ( $0.5 \text{ mol L}^{-1}$ ) for 5–15 min and then in  $\text{NaHCO}_3$  aqueous solution ( $1.0 \text{ mol L}^{-1}$ ) for another 5–15 min under vacuum ( $-0.1 \text{ MPa}$ ). This process was repeated for 1–4 times (Fig. S1). The mineralized wood chips were washed with deionized water and then freeze-dried.

### 2.3 Characterizations

The morphology of the wood samples was characterized by a field emission scanning electron microscope (SEM, SIGMA 300, ZEISS, USA). The contents of cellulose, hemicellulose and lignin were determined by the analytical procedure from National Renewable Energy Laboratory (NREL, USA). A Fourier Transform Infrared Spectrometer (FTIR, TENSOR27, BRUKER, Germany) was used to analyze

the chemical composition and functional groups of the samples with the scan range of 400–4000  $\text{cm}^{-1}$ . An automatic mercury porosimeter (Auto Pore IV 9500, Micromeritics, USA) was applied to analyze the porosity. An X-ray diffractometer (D8 ADVANCE, BRUKER, Germany) equipped with a copper source ( $\lambda = 0.154 \text{ nm}$ , 40 kV voltage, 40 mA current) was applied to characterize the crystal structure in the range of 10–80°. The mechanical properties were determined by a universal material testing machine (INSTRON 5565, USA) with a tensile rate of 1 mm/min and a compression strain of 50% at a rate of 1 mm/min. The thermal stability of the wood samples was determined using thermogravimetric (TG, TG209F3, NETZSCH, Germany) analysis under nitrogen from room temperature to 800°C at a heating rate of 10°C·min<sup>-1</sup>. Cone calorimetry testing was used to investigate the combustion of wood samples (100 mm × 100 mm × 3 mm) under a heat flux of 35 kW m<sup>-2</sup> to determine the heat release rate (HRR), total heat release (THR) and time to ignition (TTI) values of the samples. Each experiment was repeated for three times. The samples were ignited using an alcohol lamp with a 4 cm flame at an angle of 45° to ensure full contact between the sample and the flame in the burning test. The steady-state plane heat source method (Hot Disk TPS 2500S, Sweden) was used to test the thermal conductivity of the samples at room temperature. The infrared images of the samples were recorded by an infrared thermal camera (H21PRO, HIKVISION, China).

### 3 Results and Discussions

#### 3.1 Morphology and Structure

The multistep process used to prepare the composite is illustrated in Fig. 1. The native balsa wood was partially delignified by  $\text{NaClO}_2$ . After delignification, the yellowish wood block became totally white. Subsequently, the delignified balsa was impregnated with an alternating cycle of  $\text{CaCl}_2$  in ethanol and  $\text{NaHCO}_3$  in water under vacuum. The delignified balsa was impregnated with an alternating cycle of  $\text{CaCl}_2$  in ethanol and  $\text{NaHCO}_3$  in water. The  $\text{Ca}^{2+}$  reacted with  $\text{CO}_3^{2-}$  to form  $\text{CaCO}_3$  and precipitated in the wood cell walls.  $\text{CaCl}_2$  is supplied in ethanol because the solubility of  $\text{NaHCO}_3$  was low and thereby controlling the reaction rate of  $\text{Ca}^{2+}$  and  $\text{CO}_3^{2-}$ , so that the  $\text{CaCO}_3$  can distribute uniformly on the cell walls.

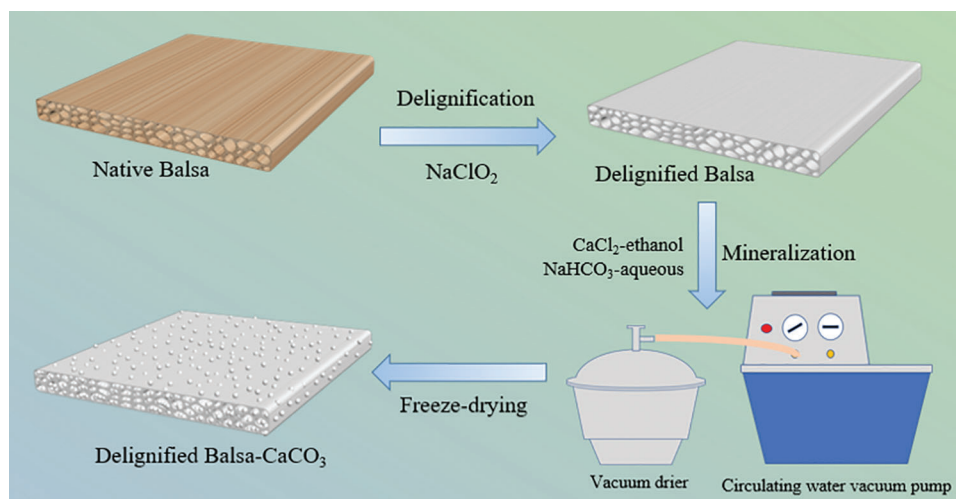


**Figure 1:** Schematic diagram of the preparation process of flame-retardant materials

Both the native and delignified balsa were mineralized with  $\text{CaCO}_3$  to prepare organic/inorganic wood hybrids. In general, the weight percent gain (WPG) increased with the processing time and the number of cycles (Fig. S1). For a single process, 10 min was enough to saturate the wood vascular with the mineral solution. Further extension to 15 min did not significantly increase the WPG. Besides, increasing the

cycle of the impregnation process (10 min) from 2 to 3 or 4 times did not clearly enhance the WPG. The WPG of delignified balsa can achieve 46.2% after mineralization by two cycles (10 min for each), which was close to the maximum value, and about three times higher than that of native balsa (15.5%). Therefore, two cycles of 10 min each time were taken as the final mineralization condition. Although the same process conditions were applied to both native and delignified balsa, the delignification significantly enhanced the diffusion rate of the mineral solution through the wood, resulting in a much higher degree of mineralization.

Native balsa processes a honeycomb-like cellular structure with thin cell walls and high porosity from the cross-sectional view, while vertically aligned fiber tracheid and vessels can be clearly seen in the longitudinal section (Figs. 2a and 2b). Delignification did not destroy the original honeycomb structure of the wood, and a large number of pores appeared in the cell walls and cell corners (Fig. 2c). The longitudinal section SEM images of delignified balsa- $\text{CaCO}_3$  (Fig. 2d) showed that spherical  $\text{CaCO}_3$  particles were uniformly distributed in the wood cavities. The removal of lignin resulted in an increase in porosity (from 79.41% to 87.51%) (Fig. 2e). The lignin content decreased from 26.1% to 12.5%, as evaluated by Klason lignin analyses (Table 1). The hemicellulose and cellulose were largely retained. To further verify the effect of delignification, the samples were characterized by FTIR (Figs. 2f and S2), where the characteristic lignin peaks at 1508, 1463 and 1420  $\text{cm}^{-1}$  (aromatic skeletal vibrations) disappeared after pretreatment. It is noteworthy that the hemicellulose-related peaks at 1738 and 1244  $\text{cm}^{-1}$  were remained, indicating the selective removal of lignin by the  $\text{NaClO}_2$  solution [28]. According to the XRD diffraction (Figs. 2g and S3) of delignified balsa- $\text{CaCO}_3$ , the  $\text{CaCO}_3$  particles are calcite crystalline. The characteristic peaks located at 23.0°, 29.4°, 36.0°, 39.4°, 43.1°, 47.5°, and 48.5°, corresponding to (012), (104), (110), (113), (202), (018), and (116) crystal planes, respectively.

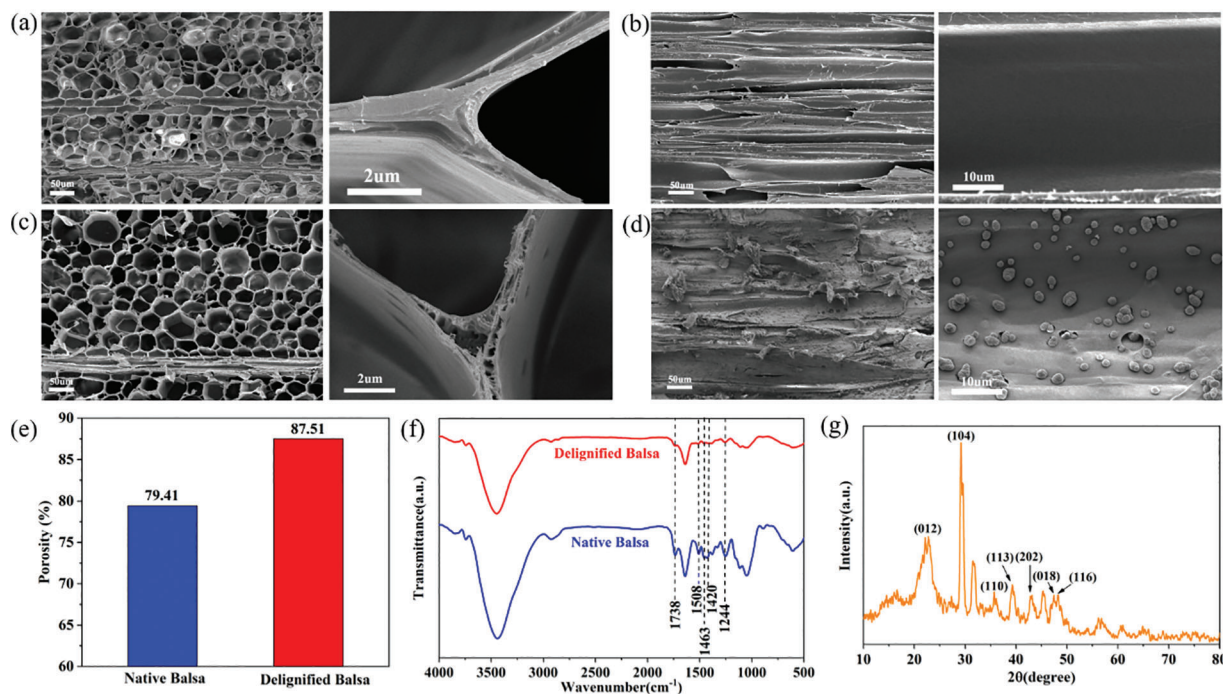


**Figure 2:** Cross sectional (a) and longitudinal section (b) SEM images of native balsa. (c) Cross sectional SEM images of delignified balsa. (d) Longitudinal section SEM images of delignified balsa- $\text{CaCO}_3$ . (e) The porosity of native balsa and delignified balsa was calculated by mercury intrusion porosimetry. (f) The FT-IR spectra of native balsa and delignified balsa. (g) The XRD diffractogram of delignified balsa- $\text{CaCO}_3$

**Table 1:** Chemical composition of the native balsa and delignified balsa

Sample	Cellulose (%)	Hemicellulose (%)	Lignin (%)
Native balsa	52.1	21.9	26.1
Delignified balsa	65.4	22.1	12.5

### 3.2 Mechanical Properties

We tested the compressive strength of the wood samples in the radial direction (Fig. 3a). At the beginning, the samples underwent a linear elastic phase at low strain, followed by a yielding phase at moderate strain and a strengthening phase at high strain during the compression process [29,30] (Fig. 3a). The compressive strength of delignified balsa was 0.81 MPa, significantly lower than that of native balsa (3.15 MPa), because the removal of lignin reduced the original strength of wood [31,32]. The compressive strength of both mineralized native balsa- $\text{CaCO}_3$  (1.19 MPa) and delignified balsa- $\text{CaCO}_3$  (3.66 MPa) increased compared to the pre-mineralized samples because the  $\text{CaCO}_3$  filled in the vascular of wood played a supporting role during compression. The elastic modulus of each sample was 19.78, 25.76, 5.72, and 10.42 MPa for native balsa, native balsa- $\text{CaCO}_3$ , delignified balsa, and delignified balsa- $\text{CaCO}_3$  (Fig. 3b), respectively. The elastic modulus of the mineralized samples was significantly higher than that of the unmineralized ones. The mineralized samples were less prone to elastic deformation also due to the calcium carbonate filling, which showed higher hardness.

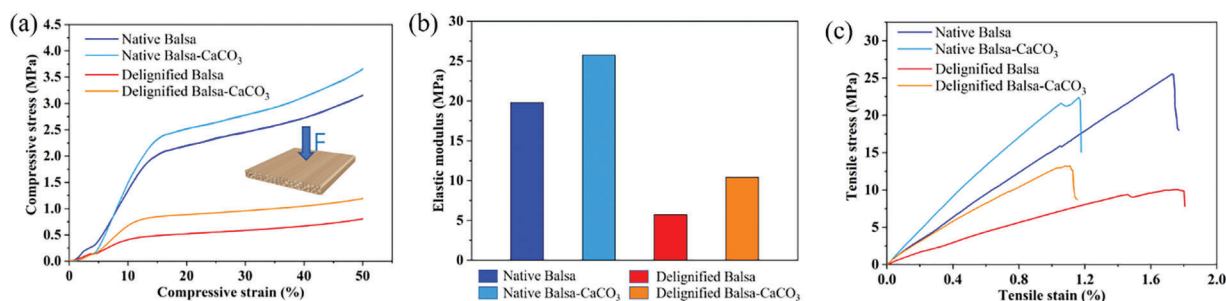


**Figure 3:** (a) Compressive stress-strain curves in the radial direction. (b) Elastic modulus and (c) tensile stress-stain curves for native balsa, native balsa- $\text{CaCO}_3$ , delignified balsa, and delignified balsa- $\text{CaCO}_3$

The tensile strength of native balsa, native balsa- $\text{CaCO}_3$ , delignified balsa, and delignified balsa- $\text{CaCO}_3$  is 25.53, 22.40, 10.04, 13.20 MPa (Fig. 3c), respectively. No significant change in the tensile strength occurred before and after mineralization. It is probably because the  $\text{CaCO}_3$  does not form bonding interactions with the fibers. The deposition of  $\text{CaCO}_3$  particles on the wood vascular is a physical process that has no significant positive effect on tensile strength.

### 3.3 Thermal Stability

The thermal stabilities of native and modified wood were evaluated by thermogravimetric analysis in nitrogen. Pyrolysis of the wood components involves two competitive pathways, which are the release of volatile products and the formation of a thermally stable carbonaceous structure. The previous studies have well documented that the pyrolysis of different wood components located in different ranges of temperature: hemicellulose, cellulose, and lignin were pyrolyzed at 200°C–260°C, 240°C–350°C, and

280°C–500°C, respectively [33,34]. The thermogravimetric curves (Fig. 4a) of mineralized samples can be divided into three stages. The first stage ranged from the initial temperature to 140°C because of the evaporation of free water and the precipitation of structural water. The second stage was from 140°C to 560°C. The main peak at a temperature corresponding to the maximum decomposition rate in the DTG curve (Fig. 4b) was ascribed to the degradation of cellulose [35], followed by a slow burnout of coke. Lignin decomposition occurred over a broader temperature range and was the main source of coke [36]. The third stage ranged from 560°C to 800°C. When the temperature reached 560°C, the  $\text{CaCO}_3$  began to be degraded and released carbon dioxide. The release of carbon dioxide was the main cause of mass loss at this stage, so the content of  $\text{CaCO}_3$  can be calculated for native balsa- $\text{CaCO}_3$  (16.2%) and delignified balsa- $\text{CaCO}_3$  (45.2%) (Table S1). The higher  $\text{CaCO}_3$  pyrolysis peak in the DTG curve also indicated a higher content of  $\text{CaCO}_3$  in the delignified balsa- $\text{CaCO}_3$  sample (Fig. 4b).

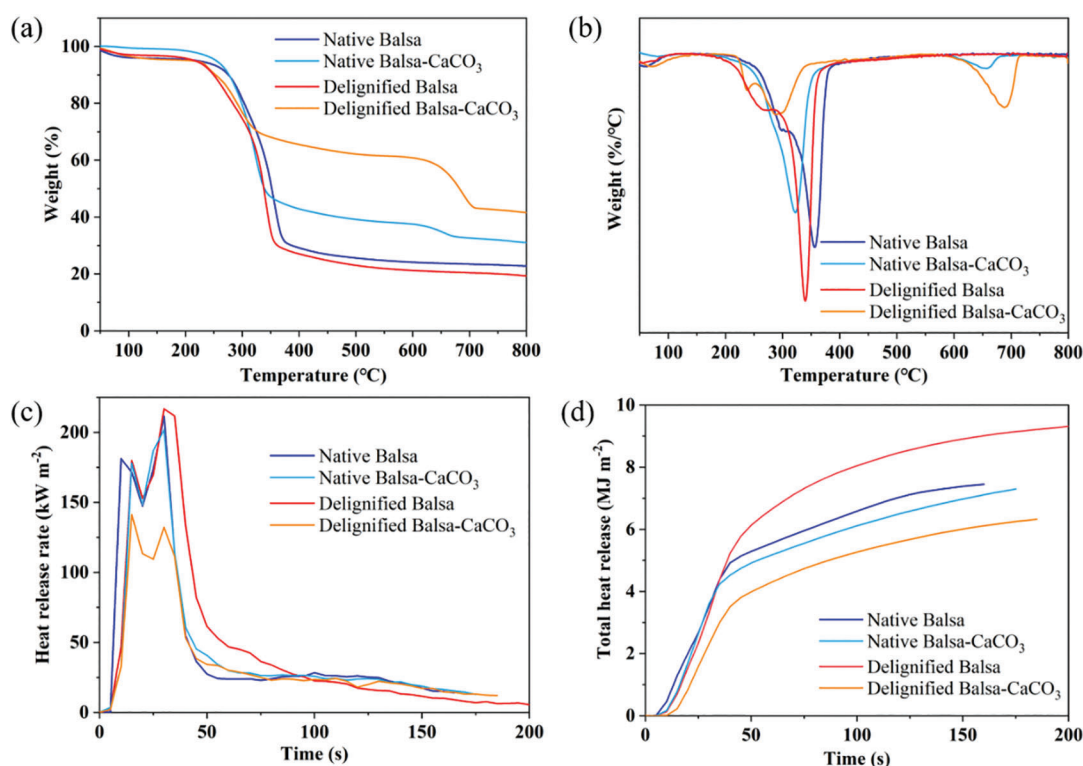


**Figure 4:** The thermogravimetric curves (a), derivative thermogravimetric curves (b), heat release rate (c), and total heat release (d) plots for native balsa, native balsa- $\text{CaCO}_3$ , delignified balsa, and delignified balsa- $\text{CaCO}_3$

At 375°C, the amounts of char were 31.3%, 44.6%, 28.4%, and 66.7% for native balsa, native balsa- $\text{CaCO}_3$ , delignified balsa, and delignified balsa- $\text{CaCO}_3$ , respectively. Likewise, when the temperature reached 560°C, the amount of char left was around 24.6%, 38.1%, 21.8%, and 61.5% for each kind of corresponding sample. Therefore, the differences in the weight of pyrolysis residue were 13.5% for native samples and 40.4% for delignified samples. According to Table S1, the gain of weight was 15.5% and 46.2% after mineralization for the native and delignified balsa. Considering the 44% weight loss of  $\text{CaCO}_3$  to  $\text{CaO}$  after pyrolysis, mineralization improved the carbon residue from lignocellulose, in

accordance with the previous study [37]. For delignified balsa, the loss of quality is greater than that of native balsa because of the removal of lignin.

### 3.4 Flame Retardant Test

Cone calorimetry was performed to test the flammability of wood samples, which are subjected to a constant heat flux of  $35 \text{ kW m}^{-2}$  from a conical radiant panel. This technique evaluates the burning behavior of materials in a fire [38]. During the tests, the samples were quickly heated and pilot ignition occurred when sufficient volatile and combustible species were released. The heat release rate (HRR) and total heat release (THR) plots are reported in Figs. 4c–4d. Table 2 shows the main parameters evaluated during the tests.

**Table 2:** Cone calorimetry data of samples

Sample	TTI <sup>a</sup> (s)	PHRR <sup>b</sup> ( $\text{kW m}^{-2}$ )	THR <sup>c</sup> ( $\text{MJ m}^{-2}$ )
Native balsa	$12 \pm 1$	$211 \pm 13$	$7.4 \pm 0.5$
Native balsa-CaCO <sub>3</sub>	$14 \pm 2$	$206 \pm 8$	$7.3 \pm 0.6$
Delignified balsa	$11 \pm 2$	$216 \pm 17$	$9.3 \pm 1.0$
Delignified balsa-CaCO <sub>3</sub>	$14 \pm 3$	$141 \pm 21$	$6.3 \pm 1.1$

Note: <sup>a</sup> TTI is time to ignition; <sup>b</sup> PHRR is peak of heat release rate; <sup>c</sup> THR is total heat release.

For native balsa samples, the first peak of HRR (PHRR) comes from the rapid combustion of volatile pyrolysis products. The HRR then declined, which might be because of the formation of a protective char on the surface, which is mainly produced from lignin. As the combustion continued, the protective char on the surface was broken down, leading to an increase in HRR to the maximum value (Fig. 4c). The following was gradual glowing and smoldering combustion with only a small amount of fragile ash remaining (Fig. S4). The removal of lignin changed the combustion behavior. The HRR curves of delignified balsa were different from that of native balsa. No protective surface char was generated for delignified balsa samples, and the PHRR was higher than that for native balsa (Fig. 4c). At the end of the test, almost no residue was left because of the absence of lignin (Fig. S4). The mineralization impacted the HRR of balsa chips differently. Mineralization of native balsa did not significantly change the HRR. However, the PHRR of delignified balsa after mineralization decreased remarkably by 40% (Fig. 4c).

The incombustible minerals embedded into wood tissues probably inhibited the release of volatile combustible materials. On the other hand, the carbon dioxide released from the pyrolysis of CaCO<sub>3</sub>, hindered the transport of oxygen to inner cellulose. The native balsa without delignification was of a low degree of mineralization, and therefore its CaCO<sub>3</sub> content was not significant enough to affect the combustion behavior. The char residue photos of mineralized samples confirmed the carbonaceous char was reinforced by CaCO<sub>3</sub>. The original fiber structure was preserved after combustion. The delignified balsa-CaCO<sub>3</sub> has more residue and a more complete wood structure due to the higher CaCO<sub>3</sub> content (Fig. S4).

THR is another important parameter to evaluate fire hazards. A good flame retardant filler is able to effectively reduce the THR of the composites [39]. As shown in Fig. 4d, the highest THR was obtained from delignified balsa. The removal of lignin made it burn with almost no char production. Without the protection of char, the carbohydrate burned violently, allowing it to release the most heat. But after mineralization, the delignified balsa-CaCO<sub>3</sub> showed significantly lower THR than the other samples. In

addition, the time to ignition (TTI) is enhanced (Table 2) because of the  $\text{CaCO}_3$  attached to the surface of the mineralized samples, which can be further improved by applying a flame-retardant coating to the surface. The smoke production rate (SPR) and total smoke release (TSR) of the samples are shown in Fig. S5, which further demonstrates their combustion behavior.

Mineralization of natural wood was performed in previous studies [14,15], but most of these methods were of low effectiveness. We significantly improved the efficiency of mineralization with  $\text{CaCO}_3$  (which can be finished within 40 min) by increasing the porosity with delignification, therefore improving flame retardancy. On the other hand, using  $\text{CaCO}_3$  as flame retardant combined with balsa wood showed advantages in mechanical properties, heat insulation, as well as cost and environmental protection, when compared to other studies [26,40,41].

We exposed the samples to open fire to evaluate their combustion properties. As shown in Fig. 5, native balsa was ignited within 3 s and produced a strong flame at 10 s. The delignified balsa is more flammable than native balsa. The native balsa- $\text{CaCO}_3$  was burned slowly and gradually self-extinguished after being removed from the flame. In contrast, delignified balsa- $\text{CaCO}_3$  produced a smaller flame at 3 s and was immediately extinguished upon removal from the flame. The above phenomenon further indicated that the filling of  $\text{CaCO}_3$  can stop the propagation of flame, and enhance the self-extinguishing effect of delignified balsa- $\text{CaCO}_3$ .

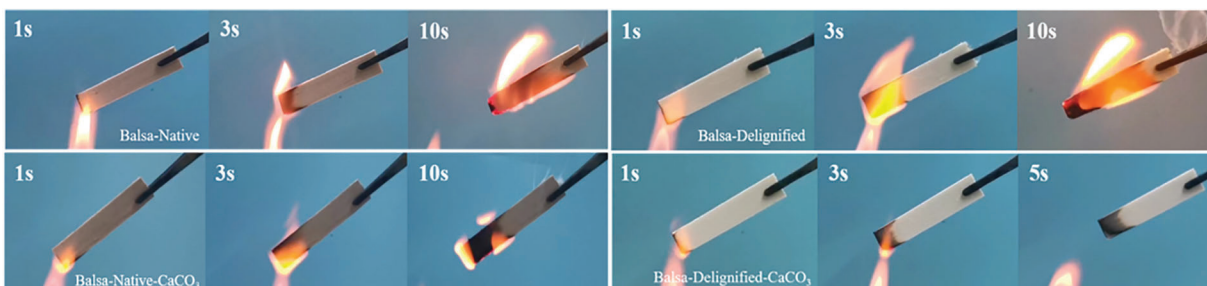


**Figure 5:** Photos during the burning test

### 3.5 Thermal Conductivity Test

To evaluate the performance of the samples in terms of energy savings, we further investigated their thermal insulation capacity along the radial direction. The samples were placed on a hot plate at  $100^\circ\text{C}$  and a top view of the temperature distribution was recorded using an infrared thermographic camera, as shown in Fig. 6a, after heating at  $100^\circ\text{C}$  for 1 min, the surface temperature of delignified balsa was the lowest ( $62.4^\circ\text{C}$ ) because the removal of lignin leads to a reduction in the connection between fibers [42]. Though the surface temperature of delignified balsa- $\text{CaCO}_3$  ( $65.4^\circ\text{C}$ ) was slightly higher than that of delignified balsa because the  $\text{CaCO}_3$  filled a large number of pores and accelerates the heat transfer rate. The temperature of balsa-native was  $70.8^\circ\text{C}$ , higher than the other samples.

Fig. 6b shows the temperature rise curves when the samples were placed on the  $100^\circ\text{C}$  hot plates. The thermal conductivity tests yielded the same conclusion as the above experiments (Fig. 6c). The thermal conductivity of delignified balsa- $\text{CaCO}_3$  is  $0.0977 \text{ W m}^{-1}\text{k}^{-1}$ , which belongs to the category of low thermal conductivity materials. Compared to other commercial insulation materials (Table 3), delignified balsa- $\text{CaCO}_3$  is also notably competitive in terms of insulation performance and is a potential insulation material [43].

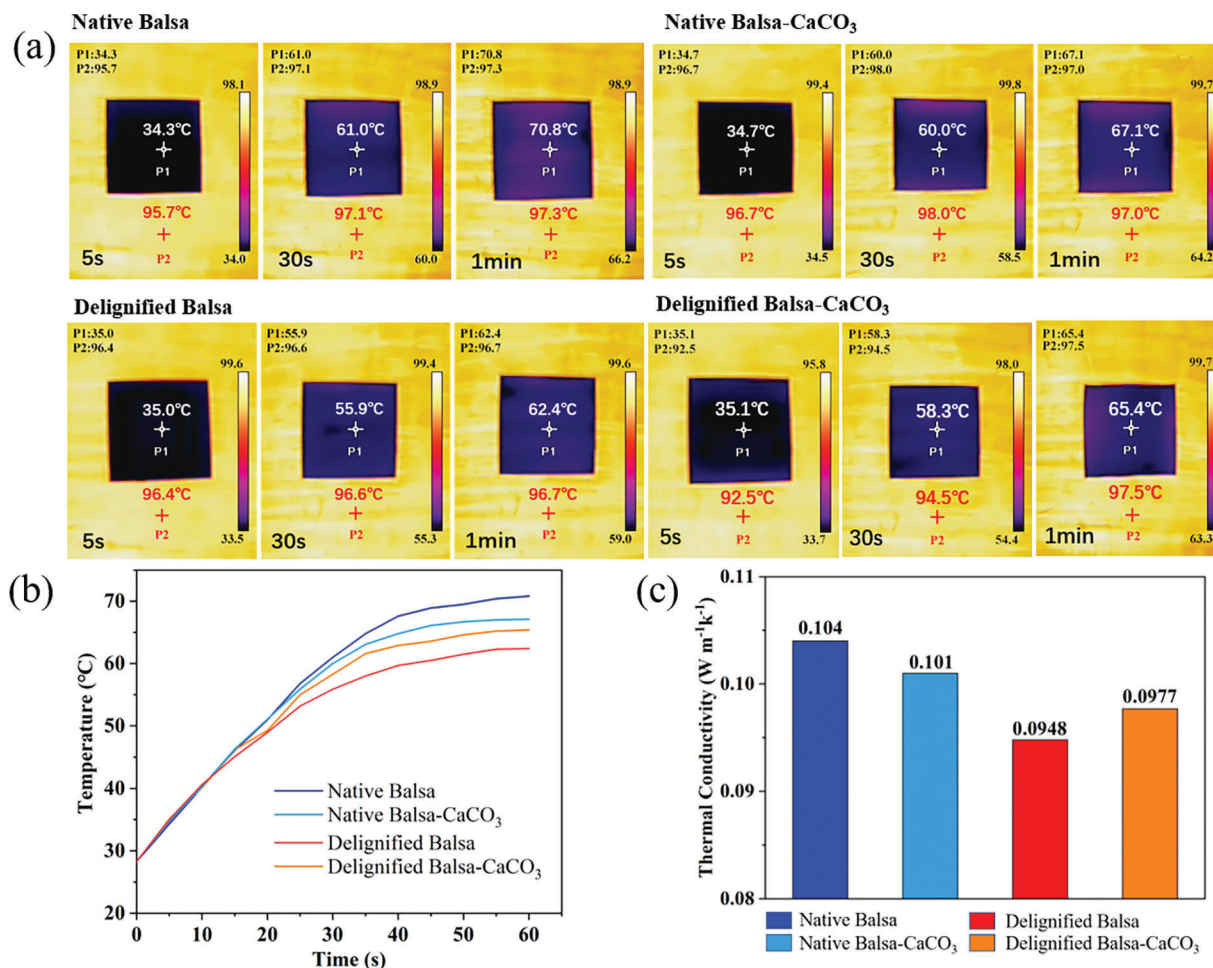


**Figure 6:** (a) The infrared thermograms of the samples when placed on a hot plate at 100°C. (b) Temperature rise curve when the samples were placed on the hot plate at 100°C. (c) The thermal conductivity of the samples

**Table 3:** Thermal conductivity of common insulation materials

Insulation material	Thermal conductivity (W m <sup>-1</sup> k <sup>-1</sup> )	Insulation material	Thermal conductivity (W m <sup>-1</sup> k <sup>-1</sup> )
Concrete	1.28	Cork	0.043
Insulating brick	1.04	Mica	0.43
Asbestos	0.15	Glass	1.09
Felt blanket	0.047	This work	0.0977

#### 4 Conclusions

In conclusion, we report a feasible method to prepare a flame retardant, self-extinguishing, thermal insulating CaCO<sub>3</sub> mineralized wood material. The delignification process in the method enhanced the porosity and wettability of the wood sample, facilitating the downstream mineralization process, that was

performed by the solute exchange. A higher degree of mineralization endowed better flame-retardant properties to the wood chips. The PHRR of delignified balsa-CaCO<sub>3</sub> (141 kW m<sup>-2</sup>) was reduced by 33% compared to the native balsa. The burning test and thermal conductivity test further demonstrated the self-extinguishing properties and thermal insulation (0.0977 W m<sup>-1</sup> k<sup>-1</sup>) of delignified balsa-CaCO<sub>3</sub>. The self-extinguishment was due to the carbon dioxide released from CaCO<sub>3</sub> during heating. It is therefore considered as an environmentally friendly flame retardant. CaCO<sub>3</sub> mineralized wood is a promising and environmentally-friendly flame retardant material [44], which can be used for energy efficient building materials or sandwich materials.

**Funding Statement:** The authors thank the Guangdong Basic and Applied Basic Research Foundation (2023B1515040013), National Natural Science Foundation of China (22108088) and State Key Laboratory of Pulp and Paper Engineering (202105) for the financial support of this work.

**Conflicts of Interest:** The authors declare that they have no conflicts of interest to report regarding the present study.

## References

1. Mao, Y. M., Hu, L. B., Ren, Z. J. (2022). Engineered wood for a sustainable future. *Matter*, 5(5), 1326–1329. <https://doi.org/10.1016/j.matt.2022.04.013>
2. Toumpanaki, E., Shah, D. R. U., Eichhorn, S. J. (2021). Beyond what meets the eye: Imaging and imagining wood mechanical-structural properties. *Advanced Materials*, 33(28). <https://doi.org/10.1002/adma.202001613>
3. Popescu, C. M., Pfriem, A. (2020). Treatments and modification to improve the reaction to fire of wood and wood based products—An overview. *Fire and Materials*, 44(1), 100–111. <https://doi.org/10.1002/fam.2779>
4. Lowden, L. A., Hull, T. R. (2013). Flammability behaviour of wood and a review of the methods for its reduction. *Fire Science Reviews*, 2(1), 4. <https://doi.org/10.1186/2193-0414-2-4>
5. Lv, S., Kong, X., Wang, L., Zhang, F., Lei, X. (2019). Flame-retardant and smoke-suppressing wood obtained by the in situ growth of a hydrotalcite-like compound on the inner surfaces of vessels. *New Journal of Chemistry*, 43(41), 16359–16366. <https://doi.org/10.1039/C9NJ04170B>
6. di Blasi, C., Branca, C., Galgano, A. (2007). Flame retarding of wood by impregnation with boric acid—Pyrolysis products and char oxidation rates. *Polymer Degradation and Stability*, 92(5), 752–764. <https://doi.org/10.1016/j.polymdegradstab.2007.02.007>
7. Wang, Q., Li, J., Winandy, J. E. (2004). Chemical mechanism of fire retardance of boric acid on wood. *Wood Science and Technology*, 38(5), 375–389. <https://doi.org/10.1007/s00226-004-0246-4>
8. He, W. T., Song, P. A., Yu, B., Fang, Z. P., Wang, H. (2020). Flame retardant polymeric nanocomposites through the combination of nanomaterials and conventional flame retardants. *Progress in Materials Science*, 114, 10687. <https://doi.org/10.1016/j.pmatsci.2020.100687>
9. Chen, S. S., Li, X., Li, Y., Sun, J. Q. (2015). Intumescent flame-retardant and self-healing superhydrophobic coatings on cotton fabric. *ACS Nano*, 9(4), 4070–4076. <https://doi.org/10.1021/acs.nano.5b00121>
10. Merk, V., Chanana, M., Gierlinger, N., Hirt, A. M., Burgert, I. (2014). Hybrid wood materials with magnetic anisotropy dictated by the hierarchical cell structure. *ACS Applied Materials & Interfaces*, 6(12), 9760–9767. <https://doi.org/10.1021/am5021793>
11. Merk, V., Chanana, M., Gaan, S., Burgert, I. (2016). Mineralization of wood by calcium carbonate insertion for improved flame retardancy. *Holzforschung*, 70(9), 867–876. <https://doi.org/10.1515/hf-2015-0228>
12. Jimoh, O. A., Ariffin, K. S., Hussin, H. B., Temitope, A. E. (2018). Synthesis of precipitated calcium carbonate: A review. *Carbonates and Evaporites*, 33(2), 331–346. <https://doi.org/10.1007/s13146-017-0341-x>
13. Morgan, A. B., Gilman, J. W. (2013). An overview of flame retardancy of polymeric materials: Application, technology, and future directions. *Fire and Materials*, 37(4), 259–279. <https://doi.org/10.1002/fam.2128>

14. Merk, V., Chanana, M., Keplinger, T., Gaan, S., Burgert, I. (2015). Hybrid wood materials with improved fire retardance by bio-inspired mineralisation on the nano- and submicron level. *Green Chemistry*, 17(3), 1423–1428. <https://doi.org/10.1039/C4GC01862A>
15. Pondelak, A., Škapin, A. S., Knez, N., Knez, F., Pazlar, T. (2021). Improving the flame retardancy of wood using an eco-friendly mineralisation process. *Green Chemistry*, 23(3), 1130–1135. <https://doi.org/10.1039/D0GC03852K>
16. Chen, C., Kuang, Y., Zhu, S., Burgert, I., Keplinger, T. et al. (2020). Structure–property–function relationships of natural and engineered wood. *Nature Reviews Materials*, 5(9), 642–666. <https://doi.org/10.1038/s41578-020-0195-z>
17. Lamm, M. E., Li, K., Qian, J., Wang, L., Lavoine, N. et al. (2021). Recent advances in functional materials through cellulose nanofiber templating. *Advanced Materials*, 33(12), 2005538. <https://doi.org/10.1002/adma.202005538>
18. Chen, C., Li, Z., Mi, R., Dai, J., Xie, H. et al. (2020). Rapid processing of whole bamboo with exposed, aligned nanofibrils toward a high-performance structural material. *ACS Nano*, 14(5), 5194–5202. <https://doi.org/10.1021/acsnano.9b08747>
19. Khakalo, A., Tanaka, A., Korpela, A., Orelma, H. (2020). Delignification and ionic liquid treatment of wood toward multifunctional high-performance structural materials. *ACS Applied Materials & Interfaces*, 12(20), 23532–23542. <https://doi.org/10.1021/acsami.0c02221>
20. Guo, W., Kalali, E. N., Wang, X., Xing, W., Zhang, P. et al. (2019). Processing bulk natural bamboo into a strong and flame-retardant composite material. *Industrial Crops and Products*, 138, 111478. <https://doi.org/10.1016/j.indcrop.2019.111478>
21. Sharma, B., Shah, D. U., Beaugrand, J., Janeček, E. R., Scherman, O. A. et al. (2018). Chemical composition of processed bamboo for structural applications. *Cellulose*, 25(6), 3255–3266. <https://doi.org/10.1007/s10570-018-1789-0>
22. Hai, L. V., Muthoka, R. M., Panicker, P. S., Agumba, D. O., Pham, H. D. et al. (2021). All-biobased transparent-wood: A new approach and its environmental-friendly packaging application. *Carbohydrate Polymers*, 264, 118012. <https://doi.org/10.1016/j.carbpol.2021.118012>
23. Jia, C., Chen, C. J., Mi, R. Y., Li, T., Dai, J. Q. et al. (2019). Clear wood toward high-performance building materials. *ACS Nano*, 13(9), 9993–10001. <https://doi.org/10.1021/acsnano.9b00089>
24. Wang, Z., Han, X., Han, X., Chen, Z., Wang, S. et al. (2021). MXene/wood-derived hierarchical cellulose scaffold composite with superior electromagnetic shielding. *Carbohydrate Polymers*, 254, 117033. <https://doi.org/10.1016/j.carbpol.2020.117033>
25. Chen, C. J., Hu, L. B. (2018). Nanocellulose toward advanced energy storage devices: Structure and electrochemistry. *Accounts of Chemical Research*, 51(12), 3154–3165. <https://doi.org/10.1021/acs.accounts.8b00391>
26. Fu, Q., Medina, L., Li, Y., Carosio, F., Hajian, A. et al. (2017). Nanostructured wood hybrids for fire-retardancy prepared by clay impregnation into the cell wall. *ACS Applied Materials & Interfaces*, 9(41), 36154–36163. <https://doi.org/10.1021/acsami.7b10008>
27. Zhang, L., Jiang, Y., Zhou, L., Jiang, Z., Li, L. et al. (2022). Mechanical, thermal stability, and flame retardancy performance of transparent wood composite improved with delaminated Ti<sub>3</sub>C<sub>2</sub>T<sub>x</sub> (MXene) nanosheets. *Journal of Materials Science*, 57(5), 3348–3359. <https://doi.org/10.1007/s10853-021-06776-3>
28. Han, X., Wang, Z., Ding, L., Chen, L., Wang, F. et al. (2021). Water molecule-induced hydrogen bonding between cellulose nanofibers toward highly strong and tough materials from wood aerogel. *Chinese Chemical Letters*, 32(10), 3105–3108. <https://doi.org/10.1016/j.ccl.2021.03.044>
29. Garemark, J., Yang, X., Sheng, X., Cheung, O., Sun, L. et al. (2020). Top-down approach making anisotropic cellulose aerogels as universal substrates for multifunctionalization. *ACS Nano*, 14(6), 7111–7120. <https://doi.org/10.1021/acsnano.0c01888>
30. Jiang, F., Hsieh, Y. L. (2014). Amphiphilic superabsorbent cellulose nanofibril aerogels. *Journal of Materials Chemistry A*, 2(18), 6337–6342. <https://doi.org/10.1039/c4ta00743c>

31. Qiu, Z., Xiao, Z., Gao, L., Li, J., Wang, H. et al. (2019). Transparent wood bearing a shielding effect to infrared heat and ultraviolet via incorporation of modified antimony-doped tin oxide nanoparticles. *Composites Science and Technology*, 172, 43–48. <https://doi.org/10.1016/j.compscitech.2019.01.005>
32. Zhang, T., Yang, P., Chen, M., Yang, K., Cao, Y. et al. (2019). Constructing a novel electroluminescent device with high-temperature and high-humidity resistance based on a flexible transparent wood film. *ACS Applied Materials & Interfaces*, 11(39), 36010–36019. <https://doi.org/10.1021/acsami.9b09331>
33. Zhang, L., Xu, J., Shen, H., Xu, J., Cao, J. (2021). Montmorillonite-catalyzed furfurylated wood for flame retardancy. *Fire Safety Journal*, 121, 103297. <https://doi.org/10.1016/j.firesaf.2021.103297>
34. Tomak, E. D., Baysal, E., Peker, H. (2012). The effect of some wood preservatives on the thermal degradation of Scots pine. *Thermochimica Acta*, 547, 76–82. <https://doi.org/10.1016/j.tca.2012.08.007>
35. Poletto, M., Zattera, A. J., Forte, M. M. C., Santana, R. M. C. (2012). Thermal decomposition of wood: Influence of wood components and cellulose crystallite size. *Bioresource Technology*, 109, 148–153. <https://doi.org/10.1016/j.biortech.2011.11.122>
36. Ren, K., Xia, Q., Liu, Y., Cheng, W., Zhu, Y. et al. (2021). Wood/polyimide composite via a rapid substitution compositing method for extreme temperature conditions. *Composites Science and Technology*, 207, 108698. <https://doi.org/10.1016/j.compscitech.2021.108698>
37. Tao, Y., Li, P., Cai, L. P., Shi, S. Q. (2019). Flammability and mechanical properties of composites fabricated with CaCO<sub>3</sub>-filled pine flakes and phenol formaldehyde resin. *Composites Part B: Engineering*, 167, 1–6. <https://doi.org/10.1016/j.compositesb.2018.12.005>
38. Schartel, B., Hull, T. R. (2007). Development of fire-retarded materials—Interpretation of cone calorimeter data. *Fire and Materials*, 31(5), 327–354. <https://doi.org/10.1002/fam.949>
39. Costa, F. R., Wagenknecht, U., Heinrich, G. (2007). LDPE/mg–Al layered double hydroxide nanocomposite: Thermal and flammability properties. *Polymer Degradation and Stability*, 92(10), 1813–1823. <https://doi.org/10.1016/j.polyimdegradstab.2007.07.009>
40. Zhang, M., Li, H., Wang, C., Wang, Z., Liu, D. et al. (2022). Performance enhancement of the poplar wood composites biomimetic mineralized by CaCO<sub>3</sub>. *ACS Omega*, 7(33), 29465–29474. <https://doi.org/10.1021/acsomega.2c03960>
41. Chen, G., Chen, C., Pei, Y., He, S., Liu, Y. et al. (2020). A strong, flame-retardant, and thermally insulating wood laminate. *Chemical Engineering Journal*, 383, 123109. <https://doi.org/10.1016/j.cej.2019.123109>
42. Song, J., Chen, C., Yang, Z., Kuang, Y., Li, T. et al. (2018). Highly compressible, anisotropic aerogel with aligned cellulose nanofibers. *ACS Nano*, 12(1), 140–147. <https://doi.org/10.1021/acs.nano.7b04246>
43. Baetens, R., Jelle, B. P., Gustavsen, A. (2011). Aerogel insulation for building applications: A state-of-the-art review. *Energy and Buildings*, 43(4), 761–769. <https://doi.org/10.1016/j.enbuild.2010.12.012>
44. Zhang, X., Wu, B., Sun, S., Wu, P. (2020). Hybrid materials from ultrahigh-inorganic-content mineral plastic hydrogels: Arbitrarily shapeable, strong, and tough. *Advanced Functional Materials*, 30(19), 1910425. <https://doi.org/10.1002/adfm.201910425>

## Supplemental Materials

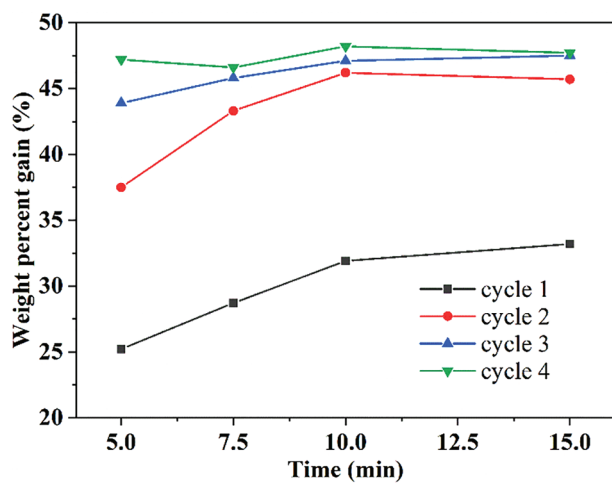


**Figure S1:** Weight percent gain of delignified balsa after mineralization

**Table S1:** The density and weight percent gain (WPG) of native balsa, native balsa-CaCO<sub>3</sub>, delignified balsa, and delignified balsa-CaCO<sub>3</sub>

Sample	Density (kg m <sup>-3</sup> )	Relative density <sup>a</sup>	WPG (%)
Native balsa	177.9 ± 3.3	0.12	~
Native balsa-CaCO <sub>3</sub>	233.3 ± 3.8	0.16	15.5 ± 1.7
Delignified balsa	117.1 ± 2.4	0.078	~
Delignified balsa-CaCO <sub>3</sub>	231.7 ± 5.8	0.15	46.2 ± 3.5

Note: <sup>a</sup> The density of the solid balsa wood is 1500 kg m<sup>-3</sup>.

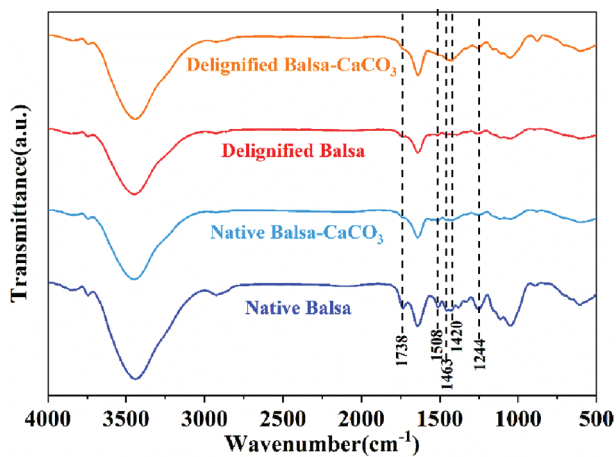


**Figure S2:** FT-IR spectra of native balsa, native balsa-CaCO<sub>3</sub>, delignified balsa, and delignified balsa-CaCO<sub>3</sub>

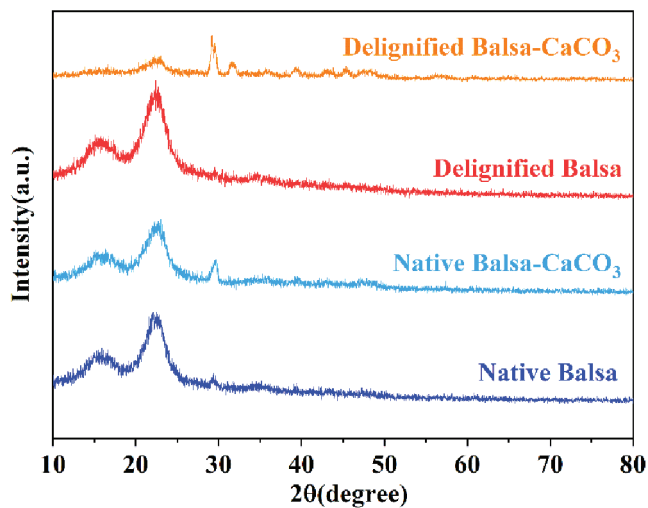


**Figure S3:** XRD patterns of native balsa, native balsa-CaCO<sub>3</sub>, delignified balsa, and delignified balsa-CaCO<sub>3</sub>

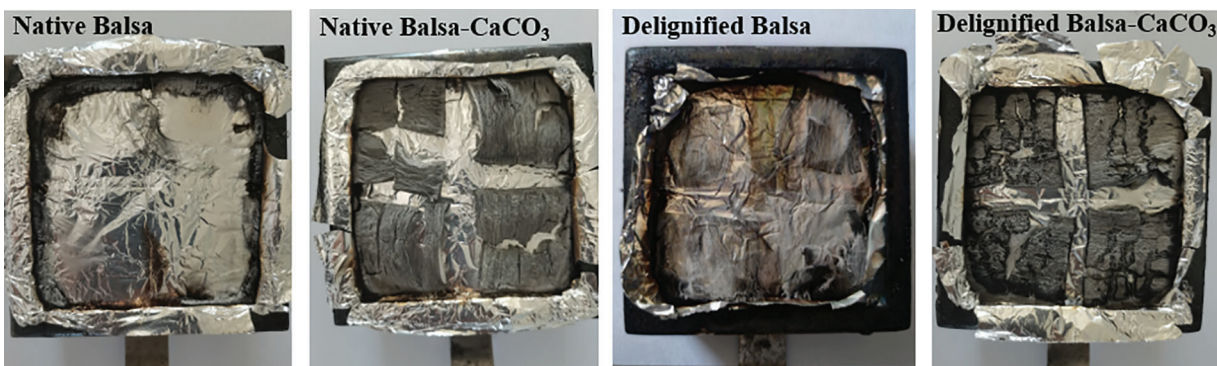


**Figure S4:** Photograph of the carbon residue

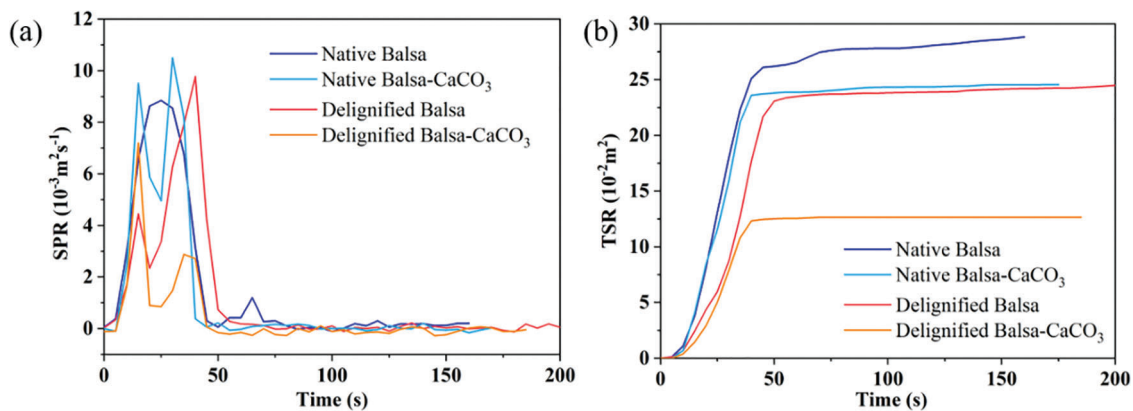


**Figure S5:** SPR (a) and TSR (b) curves for native balsa, native balsa-CaCO<sub>3</sub>, delignified balsa, and delignified balsa-CaCO<sub>3</sub>